Data fusion method to identify light elements bearing minerals from the Li-Beauvoir granite based on SEM, μXRF, and μLIBS

C Korbel, B Demeusy, Z S Kahou, Cécile Fabre, V Motto-Ros, Y Teitler, Lise Salsi, A Lecomte, I V Filippova, L O Filippov, et al.

Minerals Engineering 241 (2026) 110158

Contents lists available at ScienceDirect

Minerals Engineering

journal homepage: www.elsevier.com/locate/mineng

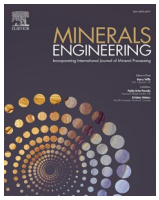

Data fusion method to identify light elements bearing minerals from the Li-Beauvoir granite based on SEM, μXRF, and μLIBS

C. Korbel [a,*], B. Demeusy [a], Z.S. Kahou [a], C. Fabre [a], V. Motto-Ros [b], Y. Teitler [a,c], L. Salsi [a], A. Lecomte [a], I.V. Filippova [a], L.O. Filippov [a], J. Cauzid [a]

[a] Université de Lorraine, CNRS, GeoRessources, UMR 7359, 54000 Nancy, France
[b] Institut Lumière Matière, UMR5306, Univ. Lyon 1-CNRS, Université de Lyon, 69622 Villeurbanne, France
[c] CSIRO Mineral Resources, 26 Dick Perry Avenue, Kensington, WA 6151, Australia

ARTICLE INFO

Keywords:
Automated mineralogy
Mineralogical mapping
μLIBS
μXRF
SEM
Lithium
Beauvoir granite

ABSTRACT

Understanding the modal mineralogy, composition, and grain properties (such as size, texture, and liberation) is crucial for optimizing mineral processing techniques, particularly in separation processes such as froth flotation, which depend on mineral surface properties. Current methods for mineralogical analysis, such as automated mineralogy tools (*e.g.*, MLA, QEMSCAN), provide detailed insights but are time-consuming and costly. Emerging techniques, including micro-X-ray fluorescence (μXRF), offer more accessible alternatives but come with limitations, particularly in spatial resolution and spectral interference between elements. This study presents a novel method combining Scanning Electron Microscopy (SEM) imaging, μXRF, and Micro Laser Induced Breakdown Spectroscopy (μLIBS) analyses, applied to the Beauvoir granite, known for its light element-bearing minerals with substantial lithium, beryllium, and fluorine contents. By calibrating μLIBS mapping with in situ Laser Ablation Inductively Coupled Plasma Mass Spectrometry (LA-ICPMS) assays and using a custom Python-based classifier for spectral data, the method achieves accurate mineralogical mapping, particularly for light element-bearing phases. Results demonstrate strong agreement with commercial automated mineralogy tools and improved classification of complex mineral phases. In this study, lepidolite was effectively identified from muscovite in coarse flotation concentrates, the first one representing about 65 % of the volume, whereas the latter represents from 7 to 16 % of the sample. This indicates the potential of the method for advancing mineral processing and metal recovery. In addition, thisstudy suggests that the low resolution of some analytical methods (~20 μm) could be improved if fused with a high-resolution mapping method, such as SEM (~1 μm). This approach is particularly relevant as light elements gain strategic importance, especially within the context of European mineral resource strategies.

1. Introduction

Quantitative information on both the modal mineralogy and grain properties (*e.g.* size, texture, and liberation size of minerals) is critical for predicting separation efficiency and identifying potential challenges in mineral processing (Fandrich et al., 2007; Gu et al., 2014; Sandmann, 2015; Sutherland and Gottlieb, 1991). Froth flotation, for instance, is a separation technique based on differences in surface properties of minerals. By selectively adsorbing surfactants onto mineral surfaces, contrasts in hydrophobicity are created, enabling their separation (Wills & Finch, 2015). Therefore, knowledge of the modal mineralogy and its textural expression, in both concentrate and tailing products of flotation, can inform strategies to improve separation efficiency (influence of gangue minerals, textures on mineral locking/liberation). To achieve this, automated mineralogy tools are increasingly used in the mineral processing research space and have significantly contributed to process optimization and improved mineral recovery (Buchmann et al., 2018; Kupka et al., 2020; Pereira et al., 2019; Vanderbruggen et al., 2021). Automated mineralogy methods use reference mineral libraries to classify each analyzed spot into a mineral phase, based on spectral/chemical matching.

Automated mineralogy is most commonly based on Scanning Electron Microscopy (SEM) commercial solutions, such as MLA, QEMSCAN, and TIMA (Gu and Napier-Munn, 1997). Mineral grain segmentation

* Corresponding author.
E-mail address: chloe.korbel@univ-lorraine.fr (C. Korbel).

https://doi.org/10.1016/j.mineng.2026.110158
Received 8 October 2025; Received in revised form 3 February 2026; Accepted 8 February 2026
Available online 18 February 2026

from Back-Scattered Electron (BSE) imaging (differences in grey level) is combined with semi-quantitative mineral chemistry from Electron Dispersive Spectroscopy (EDS). While BSE imaging with a spatial resolution of about 0.5–2 μm is quite time-effective, EDS acquisition with a typical spatial resolution of about 10–15 μm is lengthier. Minerals of interest can be specifically targeted using adapted BSE-based conditions, to obtain more spatially resolved EDS information on those (*e.g.* Bright Phase Search). However, these methods are demanding to set up: rigorous sample preparation (Pirrie and Rollinson, 2011), duration of analysis (Sutherland and Gottlieb, 1991), and access to expensive instrumentation and software.

As a consequence, emerging methods such as micro X-ray fluorescence (μXRF) are gaining increasing attention (Menzies et al., 2022; Nikonow and Rammlmair, 2017; Scheller et al., 2017; Tonžetić, 2017). These methods require minimal sample handling, are compatible with larger sample sizes (up to about 300 cm^2), and operate under vacuum or air. However, technological limitations can reduce the attractiveness of this method. Spatial resolution typically cannot go below 20 μm without extensive post-processing (Yang et al., 2022). Some manufacturers have developed apparatus able to have spatial resolution down to 5–10 μm. However, this resolution is done at the expense of excitation energy and analytical time. Such apparatus were successfully used for the characterization of concrete (Li et al., 2020). Spectral interferences between elements are common since XRF elemental analysis is based on energy dispersive X-ray fluorescence (Gallhofer and Lottermoser, 2018; Lacroix et al., 2021). Finally, the analysis is highly sensitive to the matrix composition of the sample (Flude et al., 2017). In recent years, studies on the use of Micro Laser Induced Breakdown Spectroscopy (μLIBS) mapping for the characterization of lithium-bearing rock samples have begun to emerge (Alvarez-Llamas et al., 2024; Capela et al., 2025). However, these studies are generally limited to core sample analysis or petrographic descriptions and are not constrained by analytical resolution. μLIBS has a spatial resolution of about 30 μm, which is similar to that of the μXRF. This method provides a unique access to light elements (Li, Be, B, F) which are critical for mineral classification in Lithium Cesium Tantalum (LCT) pegmatite systems. This contrasts with μXRF ($Z > 11$–13) and EDS elemental analysis limitations ($Z > 6$). On the other end, quantification is much more difficult with μLIBS as the analysis produces many spectral peaks and can be affected by very strong matrix effects.

The quantification of mineral abundances and element deportment necessitates accurate mineral classification and knowledge of mineral chemistry. In addition, grain segmentation, essential for estimating textural parameters (*e.g.* aspect ratio, mineral locking/liberation), requires good spatial resolution and is best achieved from SEM-based classification. However, the classification is done at the expense of size representativity.

Overall, SEM, μXRF and μLIBS approaches for automated mineralogy present specific, intrinsic benefits and caveats. In this context, the present work aims at developing a novel workflow based on the combination of all three methods, thus benefiting from their respective advantages while tackling their individual limitations. This workflow is applied to the Beauvoir granite Li deposit (Allier, France), which represent an ideal case study to apply as it host several types of light element (Li, Be, F)-bearing minerals (Cuney et al., 1992). The method developed relies on SEM-based BSE imaging (*i.e.* no EDS analysis), μXRF and μLIBS analyses. The μLIBS mapping is calibrated using in situ Laser Ablation Inductively Coupled Plasma Mass Spectrometry (LA-ICPMS) analysis to assess Li deportment. 2D elemental mappings from multiple instruments (here SEM-BSE imaging, element intensity maps from μXRF and μLIBS) are fused (registration and resampling) and combined for mineral classification. Results are compared to those obtained from an SEM-based commercial solution (AMICS) and from Element to Mineral Conversion (EMC) calculations on analysed aliquots. Developing a method able to combine mineralogical mapping and solve the challenge of light elements bearing phases becomes vital. This presents an even greater challenge and opportunity for innovation in the fields of economic geology and mineral processing, as light elements are increasingly becoming critical and strategic resources for European countries (European Commission, 2023).

2. Material and methods

2.1. Samples

Half diamond drill cores from various depths (from sub-surface to below 200 m) and facies (fresh and weathered granite, greisen) were sampled to provide a mixed representative sample of the Beauvoir granite. This mixed sample was crushed for beneficiation tests. Products of separation, *i.e.*, concentrate and tailing, when relevant, were sampled and cast in epoxy resin to produce polished sections of grains. From the drill core representative of the weathered granite, a thin section was produced to assess the feasibility of the method on thin sections (see Supplementary data). The selection of the grain mounted polished sections samples is summarized in Table 1.

2.1.1. Sample used to highlight the challenges and develop the method

The polished section used for the development of the method is a flotation concentrate with a particle size fraction of 10–180 μm.

Reference notches were added to the polished section to enable efficient alignment and co-registration of images acquired using various analytical methods (Fig. 1).

This sample was selected to study image alignment and co-registration due to its fine particle size distribution. The presence of smaller, well-defined crystals facilitates the detection of alignment errors, making it an ideal reference for evaluating registration accuracy. The use of such a finely structured sample thus supports the effective co-registration of images acquired through various analytical techniques.

2.1.2. Sample used for light elements analysis

The sample used to validate the developed method on the above-mentioned grain-mounted polished section, is a flotation concentrate with a particle size class of 10–500 μm. The validation is done using both LA-ICPMS and μLIBS mappings. As previously, an aliquot was cast in epoxy resin to produce a grain-mounted polished section. This sample was obtained during a flotation test for a study on the beneficiation of the Beauvoir granite. The aim of this study was to define the liberation size of the granite, as well as the technical and scientific limits of the processing scheme defined for the beneficiation of the Li deposit (Korbel et al., 2025).

This sample was chosen for light element analysis due to its coarser particle size distribution. Given the analytical methods being developed in this study, it was essential to use a sample that could be readily and successfully analyzed using both LA-ICPMS and μLIBS techniques (spot size of 30 μm).

2.2. Geochemistry

To assay the bulk geochemistry of all samples, the method from

Table 1
Samples used in this study.

Sample	Product	Purpose of the sample	Motivation
10–180 μm	Floated product	Develop the combination method using SEM and μXRF	Sample enriched in fine particles that should be effectively overlapping after co-registration of the various mappings
10–500 μm	Floated product	Addition of μLIBS	Sample with large particles than can be submitted to LA-ICPMS cross-validation for light elements analysis

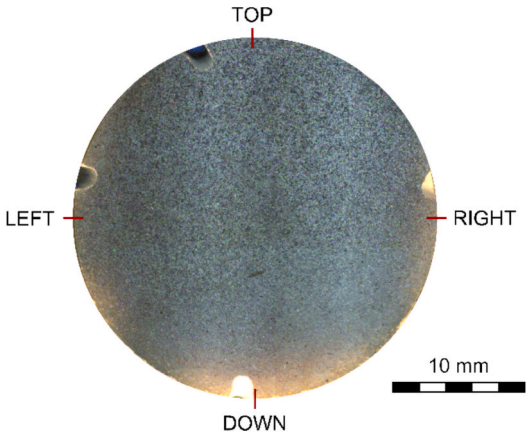

Fig. 1. Photograph of the 10–180 μm floated grain mounted polished section used for the development of the automated mineralogy method.

Korbel et al. (2024) was followed. From all studied samples, an aliquot was pulverized and assayed using a portable Niton XL3t GOLDD + spectrometer (Thermo Scientific). All Energy Dispersive X-Ray Fluorescence (ED-XRF) spectra were acquired using the Mining Hf/Ta mode as the ore contains elevated Nb and Ta contents, averaging 200 and 1000 ppm, respectively in feed samples. An analysis lasts 120 s divided in four filters used to maximize the sensitivity for the various elements (*i.e.*, Main, Low, High and Light) with a duration of 30 s each.

2.3. Characterization

Most of the characterization study was carried out in the GeoRessources research centre (Nancy, France) using analytical tools from the Service Commun de Microscopie Electronique et Microanalyse X (SCMEM) platform. μLIBS characterization is carried out at Institut Lumière et Matière of Lyon, France.

2.3.1. SEM analysis

The microscope was a Tescan Vega3 apparatus. The SEM is equipped with back-scattered electron (BSE) and two 30 mm^2 XFlash 6 Electron Dispersive Spectroscopy (EDS) detectors (Bruker, Germany). The voltage was set at 25 kV and the beam intensity at about 10nA to cover minerals bearing elements from F to U. The magnification for BSE mapping was set at 150 to optimize the scan speed and prevent from translation and rotation due the magnification.

2.3.2. μXRF elemental mappings

A thin rock section was mapped using a Bruker Tornado M4 μXRF, equipped with a Rh-tube and two 30 mm^2 EDS detectors. Analyses were carried out at a pressure of 20 mbar with the X-ray tube operating at 50 kV and 600 μA, without any filter. Analytical conditions were set up as a 20 μm-diameter spot, a dwell time of 10 ms per pixel in raster scan mode with a sample stage motion designed for 30 μm lateral resolution in the X direction and an interval of 30 μm between two consecutive lines (Y-direction), for a total acquisition time of 2 h per sample.

When needed a deconvolution of the XRF spectra can be computed. The deconvolution is carried out using the PyMca software (5.9.2).

2.3.3. LA-ICPMS

Analysis of lithium within lepidolite crystals was determined by LA-ICPMS. All measurements were acquired at the GeoRessources research centre (Université de Lorraine, France). The equipment consists of an Agilent 7900 quadrupole ICPMS coupled with a 193 nm GeoLas ArF Excimer laser (MicroLas, Göttingen, Germany). Operating parameters were set as follow: repetition rate 161 of 5 Hz, fluence of 6 J/cm^2, and laser warmup/washout of 30 s. The spot size is fixed at 30 μm. The ablated products were transported to the ICPMS using a helium flux. Specific lithium standards were used prior analyses to ensure a representative assay of the lithium content, namely NIST 610 and NIST 612 standards. The lithium concentration was computed following the procedure of Longerich et al. (Longerich et al., 1996). A total of 45 spots were done on mica crystals.

2.3.4. μLIBS

μLIBS mapping was performed using a homemade optical microscope and a Nd:YAG laser (Centurion GRM, Quantel by Lumibird) with an 8 ns pulse duration operating at 100 Hz, OPTOLySE equipment in ILM, Lyon. Plasma emission is collected through a quartz lens connected to a Czerny-Turner spectrometer (Shamrock 500, Andor Technology). The size of the laser spot for the analysis is 10 μm and the gap between two spots is set at 18 μm. The procedure followed is the one developed by Cáceres et al. (2017). Further details regarding the operational method can be found in (Alvarez-Llamas et al., 2024; Fabre et al., 2018; Nardecchia et al., 2020).

2.4. Mineralogical classification of the samples

2.4.1. AMICS: an automated mineralogy solution

The Bruker Advanced Mineral Identification and Characterization System (AMICS) software was used in combination with the Tescan Vega3 equipped with Bruker EDS spectrometers. This solution relies on spectral matching with reference spectra from a mineral library. The spectral matching accuracy can be adjusted to fine tune mineralogical classification. To optimize the acquisition time, this classification method uses a segmentation based on BSE and then each segment is chemically characterized with a small count or a fast EDS analysis. The acquired spectrum is compared to a spectral database to classify the segment.

To build the spectrum database prior to AMICS specific acquisition, a set of spectra corresponding to major and minor phases found in the ore was acquired using the same analytic conditions and a total live time of 40 s, to improve the signal/background ratio. From these spectra, a database was created and completed using spectra acquired during the specific automated mineralogy acquisition.

The final product is a false colored map with one mineral-class label per color. These mineral-class can represent single mineral and mixture of minerals depending both on the classification scheme and the study requirements. From this map, a wide range of quantitative information can be extracted, such as modal mineralogy, mineral grain size distribution, elemental deportment, mineral association, mineral liberation, etc. This solution is showing increasing interest due to its possible use both with μXRF and SEM-EDS equipment (Barker et al., 2021; Jiao et al., 2020; Zhang et al., 2019). In this study, AMICS is used to compare the mineralogical classification done by the developed method (modal mineralogy, minerals textures) on both thin section (see Supporting Data) and grain-mounted polished section.

2.4.2. MARCIA Python library: A homemade manual classifier

The MAsking spectRosCopIc dAtacube (MARCIA) Python library is a manual classifier developed for μXRF hypercubes (Meyer and Cauzid, 2021). However, this classifier can be used to process any type of hypercubes (μXRF, SEM, μLIBS, images, etc.). The classification is achieved by defining phases masks, *i.e.*, mineral masks, which are combination of elemental intensities (normalized to 100 % or non-normalized) in the global spectrum. Based on this classification, a false colored map can be plotted. Example of a classification computed using the MARCIA python library for the beneficiation study of a phosphate ore was done by Boucif et al. (2024).

Based on the combination of the SEM-BSE, μXRF, and μLIBS mapping methods, false colored mineralogical maps were produced using the MARCIA Python library. From these false colored maps, modal mineralogy of the samples and grain size distribution of a given mineral can be

assessed. Further statistics computation such as mineral association and liberation degree might be developed in the future. Yet, the interest in this specific study is to compare (i) mineral textures and (ii) modal mineralogy computed by the two methods, *i.e.,* MARCIA and AMICS.

2.5. Element to mineral conversion (EMC)

The Element to Mineral Conversion (EMC) method is based on solving a set of linear equations between element and mineral grades. Given a sample, this can be translated by the Equation (1):

$$C \times m = e \Leftrightarrow \begin{bmatrix} c_{11} & \cdots & c_{1n} \\ \vdots & \ddots & \vdots \\ c_{n1} & \cdots & c_{nn} \end{bmatrix} \times \begin{bmatrix} m_1 \\ \vdots \\ m_n \end{bmatrix} = \begin{bmatrix} e_1 \\ \vdots \\ e_n \end{bmatrix} \quad (1)$$

Where *C* is the matrix of the chemical composition of minerals, called conversion matrix, *m* is the vector of modal mineralogy (unknown vector), and *e* is the vector of element grades of the sample; Eq.1.

In this study, the C matrix was determined based on LA-ICPMS for overall geochemistry and lithium assays. The e vector is determined using ED-XRF. Finally, the linear equation is solved using Python least squares function from the SciPy package.

The EMC method is used to convert elemental assays into modal mineralogy for samples submitted to separation processes. Based on this conversion, modal mineralogy can be compared to the ones obtained with mineralogical classification of polished sections. This comparison should increase or discuss the robustness of the mineralogical observations given by AMICS and MARCIA. However, the EMC method presents certain limitations. In its conventional form, it is computationally feasible only when the dimension of vector *m* matches that of vector *e*. Some researchers are exploring predictive approaches that remain effective even when the vector *e* has fewer components than *m* (Tolosana-Delgado et al., 2011).

3. Results

3.1. The Beauvoir granite as a perfect case study to study the characterization of light elements

The Beauvoir granite is a peraluminous, phosphorus-rich rare metals granite located in Allier, France. This granite is a one of the latest intrusions from the Variscan orogenesis. It contains substantial amounts of Li-bearing (lepidolite, amblygonite), F-bearing (fluorite, topaz), and Be-bearing (Be-phosphate) minerals (Cuney et al., 1992; Kosakevitch, 1976) and is therefore characterized by elevated lithium, fluorine, and beryllium contents (Charoy, 1999; Pollard, 1995). The chemical formula, qualitative mineral abundance, and associated light elements are summarized in Table 2.

The five above-mentioned minerals can represent up to 35 % of the minerals present in the Beauvoir granite (Table 2). Hence, developing a method to detect and qualitatively distinguish enrichment in light elements appears essential for automated mineralogy applied to such mineral associations.

Table 2
Light element bearing minerals and their abundance in the Beauvoir granite according to (Aubert, 1969; Cuney et al., 1992).

Mineral	Formula	Abundance	Discriminating elements
Lepidolite	$K(Li,Al)_3(Si,Al)_4O_{10}(F,OH)_2$	10 to 25 %	Li-F
Amblygonite	$(Li,Na)AlPO_4(F,OH)$	Several volume percent	Ca/Na-Li
Be-phosphate	$CaBe(PO_4)(F,OH)$	~1 %	Be-P
Fluorite	CaF_2	~1 %	Ca-F
Topaz	$Al_2SiO_4(F, OH)_2$	1 to 5 %	F

The presence of muscovite, formed by hydrothermal weathering (Kahou et al., 2024), together with lepidolite, represents a significant challenge for effective mineral classification. Although both minerals have close geochemistry and crystal structure, only lepidolite carries elevated concentrations of lithium. It is therefore crucial to decipher these two minerals through the workflow, especially in the perspective of selective mineral processing.

3.2. The challenge of data fusion with multiple mapping techniques highlighted by the 10–180 μm floated sample

Further details on the data fusion method developed for thin sections can be found on supplementary data and in previous studies (Korbel et al., 2025, 2024).

3.2.1. Analytical volume

As highlighted in a previous study, one advantage of lepidolite from the Beauvoir granite is its specific enrichment in rubidium (Korbel et al., 2024). Hence, this element can be used as a proxy (i) for lithium quantification (Bradley et al., 2017; Lagache and Quemeneur, 1997; Neukampf and Ellis, 2025) and/or (ii) for the identification and classification of lepidolite in thin sections, even for samples bearing K-feldspar (Fig. S1, S2 and S3). Furthermore, the Beauvoir granite is also enriched in several heavy minerals such as cassiterite (Sn), columbite group minerals (Nb,Ta), and microlite (Ta). However, the classification of all these heavy elements-bearing minerals faces several obstacles when considering only the information provided by elemental mappings measured for grain mounted polished sections.

Fig. 2 displays the BSE grains mapping (Fig. 2a) along with μXRF mappings of two heavy elements of interest Rb, for lepidolite identification (Fig. 2b), and Sn, for cassiterite identification (Fig. 2c). The maps are compared visually rather than quantitatively due to (i) differences in resolution and (ii) translation and rotation discrepancies between datasets. Without accurate image alignment, a pixel-by-pixel comparison is not achievable.

The Rb intensity map shows no correlation with the grains identified from BSE as lepidolite and the Sn map highlights more Sn-rich grains than effective in the sample (bright grains in BSE). It is therefore impossible to use these raw intensity maps from μXRF. The elevated background noise observed both in the Rb and Sn raw maps result from (1) the high background noise and (2) the depth of information. The analyzed volume and depth depending on the X-ray energy emitted by the excited atom is displayed in Fig. 3. In a siliceous matrix, X-ray with energies above 5 keV are emitted from deeper than 10 μm, which can imply the analysis of several grains in depth, on the same location.

Therefore, tin having photon energies ranging from 25.271 keV for its Kα emission line to 3.444 keV for its Lα emission line, emission from depths greater than 1000 μm can occur (Haschke, 2014; Kaskes et al., 2021). This explains the high number of grains identified in the Sn μXRF mapping compared to the concentration of Sn in the ore. To overcome this limitation, it is necessary to run a deconvolution of the μXRF spectra, in order to make use of low energy X-ray lines.

3.2.2. Deconvolution of XRF signal

Based on the deconvolution carried out, the Kα and Lα emission lines of rubidium and tin are identified and extracted from the overall XRF spectrum (Fig. 4). Based on this deconvolution, elemental mappings according to specific emission lines can computed. These maps are displayed in Fig. 5. Clear link between the emission energies and the obtained mappings can be done. In the case of rubidium, the Kα emission line is characterized by a high energy of about 15 keV. Compared to Fig. 3, in a siliceous matrix, the depth of information can exceed 1000 μm. Hence, the obtained mapping, compared to BSE imaging, has a noisy aspect. This aspect, once again, is related to the signal from grains at depth and to the high background noise. On the contrary, the Lα atomic emission line of rubidium as an energy of about 1.7 keV. Such energies

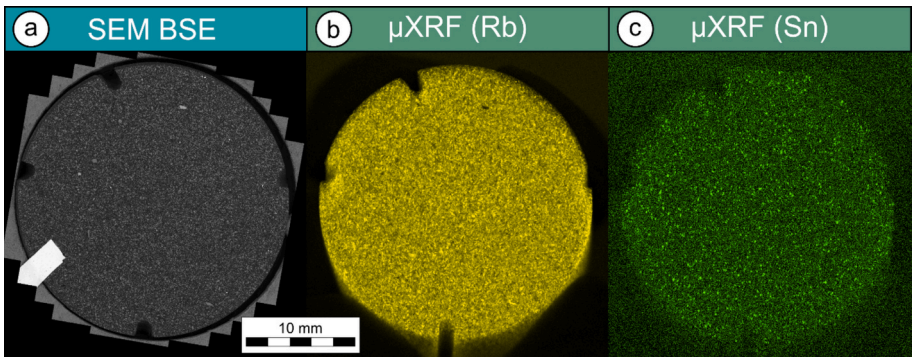

Fig. 2. (a) BSE image of the polished section along with (b) Rb and (c) Sn elemental mappings.

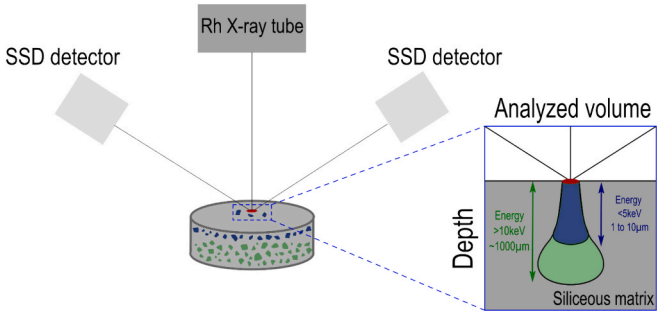

Fig. 3. µXRF analyzed volume in a siliceous matrix depending on the photo X-ray electron energy. Figure adapted from data of (Haschke, 2014)

are low for the analytical procedure, namely a low vacuum of about 20 mbar and the use of SDD spectrometers. Such conditions exhibit limits for the detection and quantification of such photo X-ray electron energies. Thus, the mappings obtained exhibit analytical noise.

Nonetheless, mappings are slightly different considering tin. If the same observation can be done for the Kα emission line, with an energy of about 25 keV, the deconvolution method shows characterization improvement when considering the Lα emission line of tin. It means that taking into account photo X-ray electron energy, *i.e.*, 3.4 keV, mapping allows to reduce the analytical volume (Fig. 3) and identify some Sn grains located on the surface of the polished section.

Hence, the number of tin-bearing grains in the polished section is greatly reduced and their apparent distribution matches that obtained BSE imaging (bright grains in Fig. 5a' and 5e).

3.2.3. *Light elements diffusion and µXRF analytical spot*

Thus, when not corrected through signal deconvolution or to ensure a simple classification method based on major elements mappings only, lighter elements were used, such as Si, Al, K, Ca, P, etc. However, these elements, based on µXRF methods, can be affected by X-ray diffusion within the sample (Potts, 1992; Tjallingii et al., 2007). Furthermore, the effect of the analytical spot and lateral step of the device can further impact the quality of the elemental maps for grained mounted polished sections. Fig. 6 displays a hypothetical "model" grain in the grain mounted polished section, which has been submitted to SEM-BSE imaging and µXRF analysis, shown with the K elemental mapping (Fig. 6a

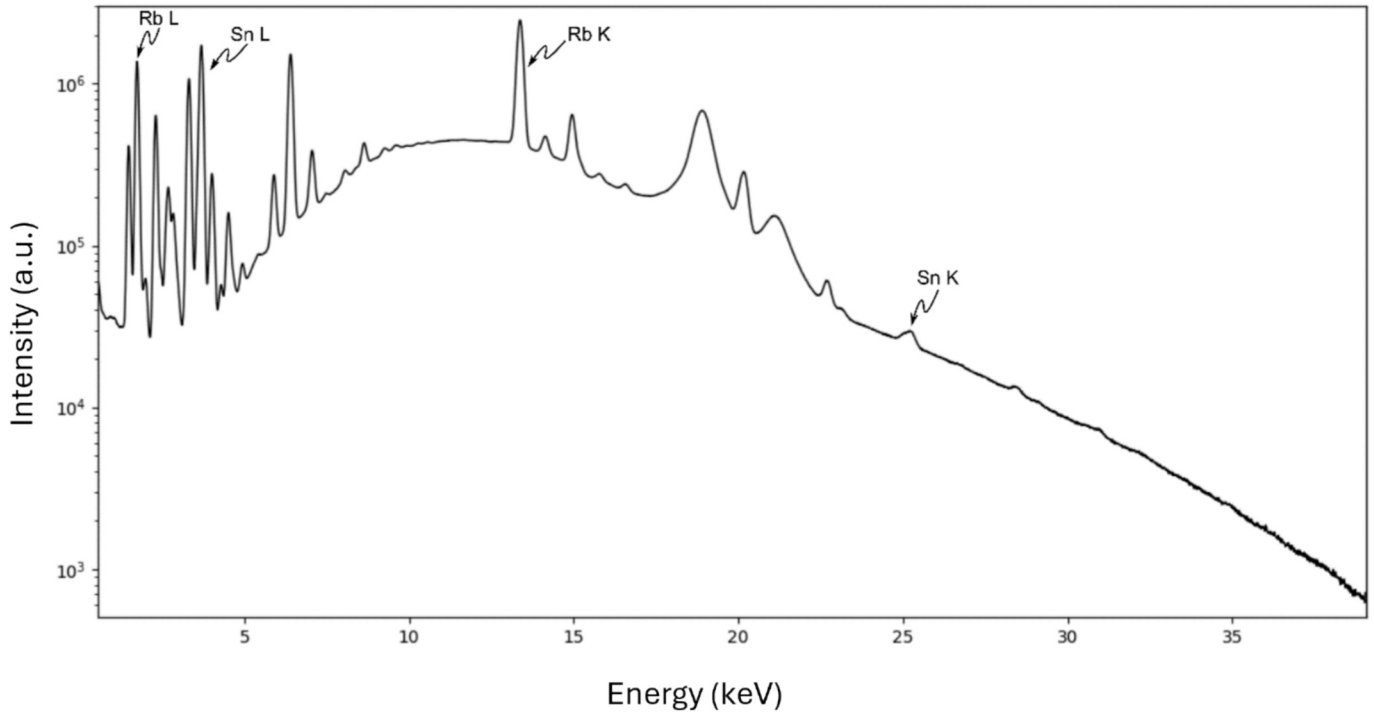

Fig. 4. Overall spectrum of the µXRF analysis of the grain mounted polish section studied. The deconvolution carried out using PyMca allowed to detect the different emission lines of rubidium and tin.

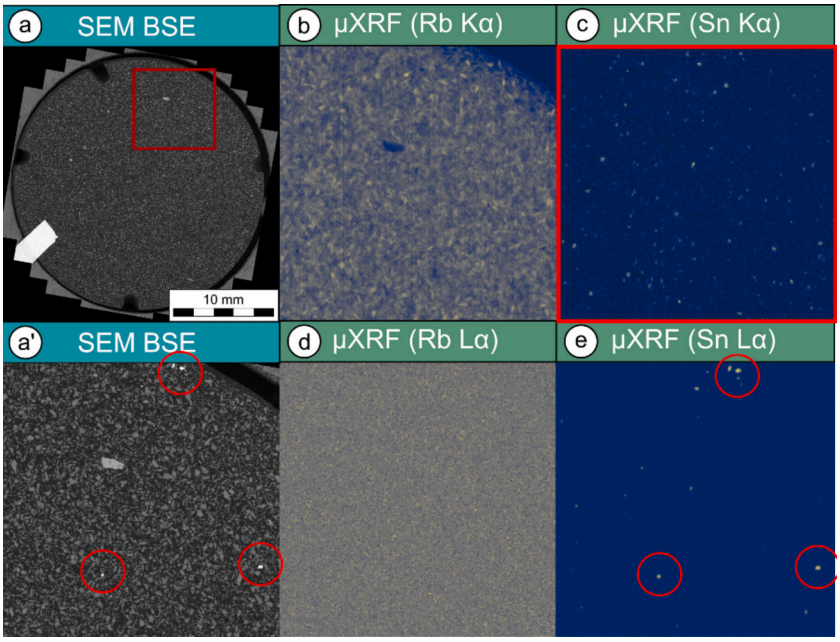

Fig. 5. (a) BSE image of the polished sections with the red square showing the zoomed area. (a') BSE image of the zoomed area. Elemental mappings of the zoomed area considering (b) the Rb Kα = 13.396 keV emission line, (c) the Sn Kα = 25.271 keV emission line, (d) the Rb Lα = 1.692 keV and (e) the Sn Lα = 3.663 keV. Red circles highlight cassiterite grains effectively identified in the BSE and Sn Lα mappings. The red square in the Sn Kα highlights possible grains at depth within the sample. (For interpretation of the references to colour in this figure legend, the reader is referred to the web version of this article.)

and 6b). This model grain is used to show the effects of the different analytical measurements, *i.e.,* SEM-BSE and μXRF, on the mappings of this grain. Since SEM is a widely used apparatus for morphological analysis and having a micrometer resolution (Ortiz Ortega et al., 2022), the hypothesis is made that a model particle, with its size ranging from 10 to 200 μm, will have the same shape displayed using SEM-BSE imaging as its current one in the grain mounted polished section. However, the same model grain observed using the potassium elemental μXRF map will appear coarser and its shape might be different (Fig. 6b). Such observation can be related to the analytical volume of the μXRF analysis and to the diffusion of X-rays in the sample. Such effects can impact the total area that would be associated to the particle when using manual classification based on the X-ray signal.

The purpose of the developed data fusion method is to overcome

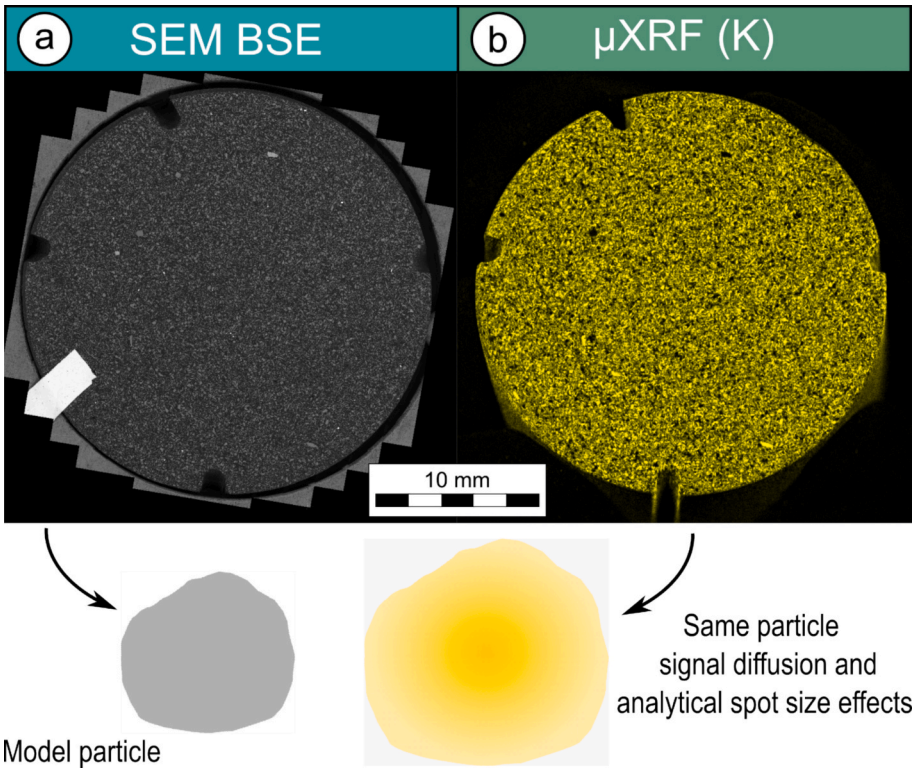

Fig. 6. (a) BSE image of the polished section and a zoom to a model grain and (b) K elemental mapping and a zoom to the same model grain.

these strategic limitations and enhance spatial resolution by integrating both analytical techniques. Specifically, by overlaying SEM-BSE and μXRF maps, minerals can be pre-classified using the BSE signal, and individual grains can then be isolated based on their μXRF response, guided by their BSE-defined outlines.

Nonetheless, several challenges remain in developing this method: (i) to ensure compatibility with the MARCIA mineralogical classification code, the datasets must have identical dimensions (*i.e.* same width and height); (ii) translation and rotation between BSE and μXRF datasets must be corrected.

3.3. The specific challenge of the Beauvoir granite: distinguishing lepidolite and muscovite

3.3.1. 10–500 μm flotation concentrate geochemistry

The geochemistry of the concentrate sample, obtained by portable XRF, is provided in Table 3. The lithium content, estimated from the Rb content (Korbel et al., 2024) is 2.97 %Li_2O, which is a concentration commonly achieved through flotation (Table 3).

3.3.2. μLIBS and LA-ICP-MS analyses of the 10–500 μm floated sample

As mentioned above, Rb mapping should be a pivotal element to decipher muscovite and lepidolite but cannot be exploited in the operating conditions used. Thus, a smaller portion of the sample was submitted to μLIBS analysis to obtain elemental maps of light elements such as Li, Be, F, etc. The mapping of the Li I 670.7 nm emission line is displayed in Fig. 7. This figure highlights that lithium can effectively be detected in the sample. Furthermore, lithium seems to be distributed at two different concentration levels: not concentrated, *i.e.*, intensities below 10,000 (arbitrary unit), and highly concentrated, *i.e.*, intensities above 40,000 (Fig. 7 – bar plot). However, LIBS technologies are known to be highly sensitive to the presence of lithium, since some authors were able to set limits of quantification down to 2–20 pg of Li using the same atomic lines for rock and liquid samples, respectively (Berthou et al., 2024; Fabre et al., 2002; Lee et al., 2011). Thus, in order to compare these measured intensities to a lithium concentration, LA-ICPMS measurements were carried out to calibrate the μLIBS lithium analysis. The location of the spots is displayed on Fig. 7.

Lithium concentrations assayed on the different locations are plotted on Fig. 8. It shows that the lithium concentration in lepidolite grains is homogeneous, with a mean value of about 6.25 %Li_2O (Fig. 8). Therefore, this study highlights that μLIBS can effectively record lithium concentration and that the high intensities acquired using this method can be related to effective lithium concentrations in the sample assayed using LA-ICPMS.

Thus, μLIBS can be an efficient method to map light elements, such as Li, Be and F, and is a clue to effectively separate muscovite from lepidolite. The combination of this method along with μXRF and SEM imaging is discussed in the following section.

3.4. Integrated solution for mineralogical classification of the 10–500 μm sample

3.4.1. Homography

To be able to perfectly overlay images, considering resolution, rotation and translation differences, the determination of the homography matrix between the two images is necessary. This matrix is defined in Equation (2).

$$\begin{bmatrix} x_{SEM} \\ y_{SEM} \\ 1 \end{bmatrix} = \begin{bmatrix} H_{11} & H_{12} & H_{13} \\ H_{21} & H_{22} & H_{23} \\ H_{31} & H_{32} & H_{33} \end{bmatrix} \begin{bmatrix} x_{\mu XRF} \\ y_{\mu XRF} \\ 1 \end{bmatrix} \quad (2)$$

Where, (x_{SEM}, y_{SEM}) are the coordinates of a reference point in the mapping obtained by SEM, ($x_{\mu XRF}$, $y_{\mu XRF}$) the coordinates of the same reference point in the mapping obtained by μXRF, and H_{ij} the elements of the homography matrix.

This function (findHomography from the OpenCV Python package) allows, from a source image and a target image, to resize the first image to the same dimension (and resolution) as the target image, while correcting for translation and rotation effects between the two images. This function requires a minimum of four reference points to calculate the homography matrix. To date, the use of such method to combine analytical methods has been identified once in the literature (Maragh, 2021). One major advantage of this method is to end-cut particles in the μXRF mapping thanks to the BSE mapping. This step allows for a greater flexibility in the μXRF-based classification thresholds, as noise signal has been artificially removed by the end-cut.

This method is similar to the co registration procedures applied to multi sensor datasets integrated with aerial imagery. Such techniques are widely employed for the quantitative monitoring of ground deformation and slope instability phenomena. In this context, ground control points (GCPs) are typically used to constrain the co registration process and ensure that all derived products share a consistent spatial reference and resolution (Ayoub et al., 2009; Behling et al., 2014).

3.4.2. Mineralogical classification of the sample using SEM-BSE, μXRF, and μLIBS

The mineralogical classification of the sample, conducted using the method developed with SEM and μXRF and adding μLIBS mapping to obtain elemental maps of light elements such as Li, Be, F, etc., is presented in Fig. 9 (b and d). The mapping shows that the sample is mainly composed of lepidolite. The grains of lepidolite can be completely liberated or present as mixed particles (Fig. 9). Various sizes of lepidolite grains are identifiable in the concentrate (Fig. 9).

The same area was mapped and classified using the SEM (BSE + EDS)-based AMICS commercial solution. It is displayed twice for better comparison of the results (Fig. 9 a and c). Mineral classification based on μXRF- BSE combination only shows some limitations, including (1) unclassified pixels and (2) wrongly classified pixels, particularly for K-feldspar and lepidolite mixed particles (Fig. 9a and 9b). Whereas better overall classification is obtained when adding μLIBS mapping. Mixed particles can be identified and distinction between lepidolite and muscovite seems effective as compared to AMICS classification method (Fig. 7, Fig. 9c and 9d). This shows the accuracy of the developed method for (i) identifying the different minerals phases and (ii) the different textures present in the samples. Interestingly, if SEM and μXRF is able to provide first information on the sample composition, adding LIBS mapping definitely improves the mineralogical description of the sample.

Table 3
Geochemistry of the floated product, obtained by ED-XRF. Lithium content is estimated following method described in (Korbel et al., 2024).

Li_2O (%)	SiO_2 (%)	Al_2O_3 (%)	K_2O (%)	Sn (ppm)
2.97	59.08	24.70	7.60	1197

4. Discussions and perspectives

4.1. Error related to the reference points selection

The reference points used to calculate the homography matrix (Equation (2) can be identified using grains with characteristic features. However, an error can occur in the μXRF image, as the measured intensity can diffuse into the sample resin. For this reason, four notches were made in the sample presented. Identifying the angle of the notch in relation to the contour of the polished section is easy, reliable and achievable at any resolution of the equipment (ranging from μm to tens of μm).

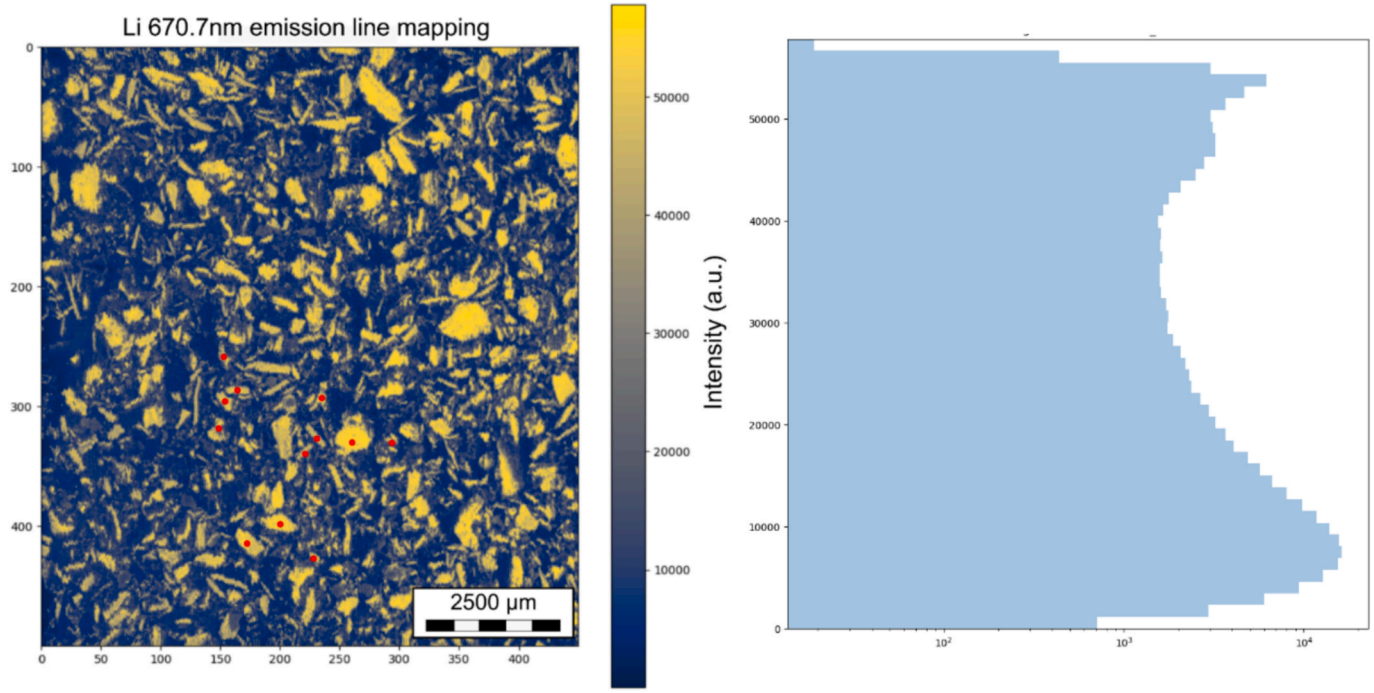

Fig. 7. Li 670.7 nm emission line mapping obtained through µLIBS. The color bar represents the intensity measured. The red dots represent the in-situ LA-ICPMS analyses carried out prior to µLIBS measurements. The bar plot displays the distribution of Li 670.7 nm emission line intensities. (For interpretation of the references to colour in this figure legend, the reader is referred to the web version of this article.)

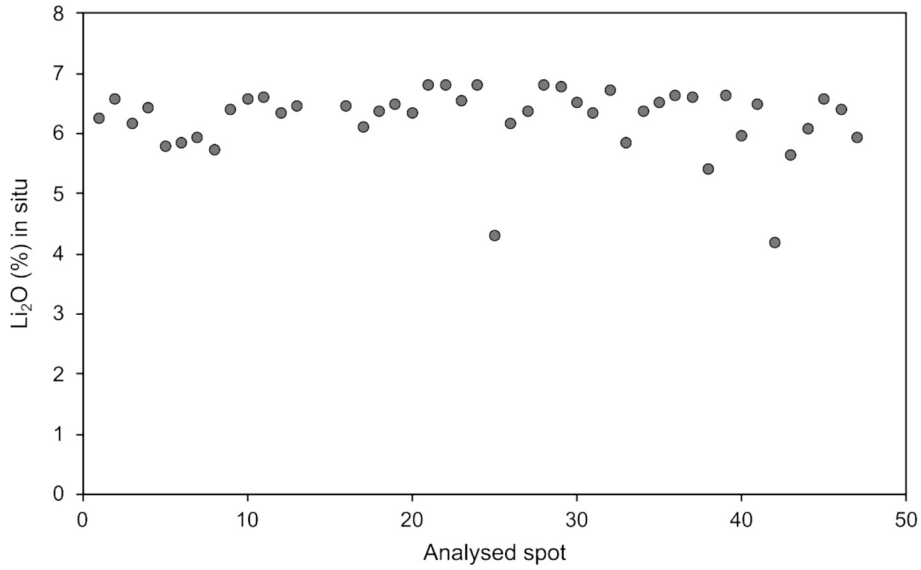

Fig. 8. Lithium concentration measured by LA-ICPMS at location described in Fig. 11. Mean lithium concentration is of about 6.25 %Li_2O and standard deviation of 0.55.

The identification of notches from the SEM is illustrated in Fig. 10a. The position (X,Y) of each notch was measured in mm using the SEM software. Using the routine SEM mapping file, it is possible to know the minimum and maximum positions analyzed (in mm), in X and Y. Knowing the maximum and minimum sizes of the mapping (in mm), in X and Y, as well as the resolution of the image obtained (in pixels), in X and Y, it is possible to automatically reposition the position of the notches (blue dots).

The same methodology can be applied to the X-ray micro-fluorescence spectrometer. Once the reference points have been identified (Fig. 11a), the homography matrix can be calculated (Fig. 11c). Without this methodology, BSE images and µXRF mappings have large differences in resolution, so that small errors in landmark selection can have significant influence on data correlation, as illustrated in Fig. 11b.

4.2. Modal mineralogy

The modal composition of the sample obtained from EMC, *i.e.*, calculated from bulk rock mineral chemistry, is compared to modal abundances obtained from the AMICS and MARCIA techniques (Table 4). While good agreements are obtained for the quantification of lepidolite, quartz and K-feldspar, limitations are observed for the

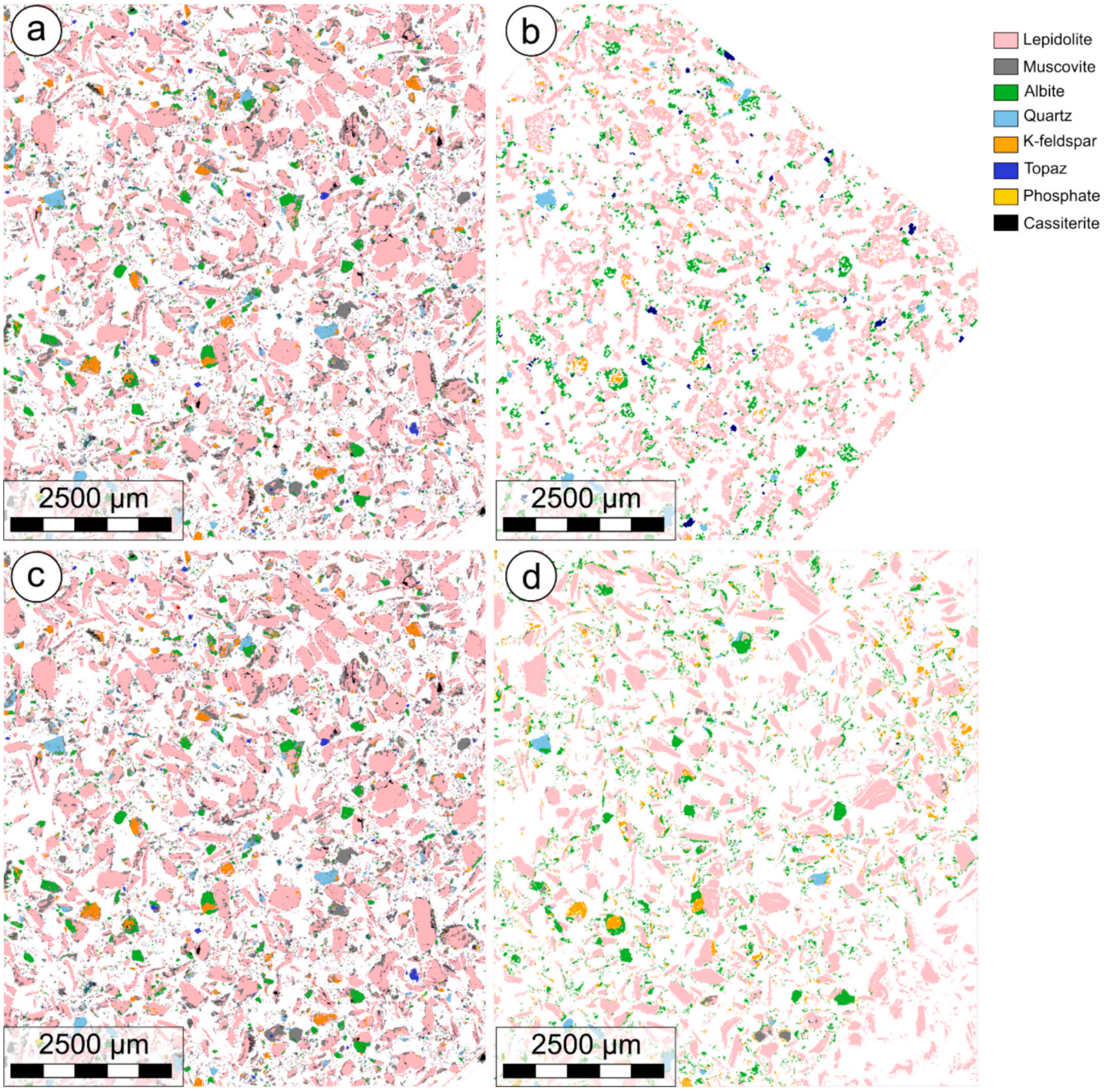

Fig. 9. Same portion of the polished section classified using (a and c) AMICS software, (b) MARCIA classification with the combination of BSE and µXRF mappings only and (d) MARCIA classification with combination of BSE, µXRF and LIBS mappings.

quantification of albite and topaz (Table 4). This may be related to the semi-quantitative determination of sodium content by ED-XRF, which can lead to erroneous quantification of albite content in the sample. Furthermore, a large quantity of minerals is attributed to topaz by matrix calculation (Table 4). This may be related to the particular chemistry of this mineral, *i.e.*, Al, Si, F, which is quite similar compared to feldspars (albite and K-feldspar) and the low quantity of sodium determined by ED-XRF. One approach to determine the limit of these calculations would be to analyze the samples by ICP-MS to obtain reliable quantification of sodium and compare the results obtained. Facing such challenges, some authors also combined chemical assays with semi-quantitative XRD (Parian et al., 2015). Moreover, the question of reconstruction between mass percentage and surface percentage can be raised here. Lepidolite having a high shape factor, the grains of this phyllosilicate can preferentially sediment according to their basal face during the resin embedding of polished sections. Such limitations have been identified by Jeong for samples without specific preparation (Jeong, 2008). This can lead to an overestimation of the surface percentage of lepidolite and may also be the cause of quantification differences between the three methods and more specifically between mappings quantification methods, *i.e.*, MARCIA and AMICS, and EMC quantification method.

In the case of automated mineralogy methods, on overall good agreement in obtained between the two methods, except for albite that seems to be impacted by the sensitivity of µXRF, which lead to an overexpression of this mineral in the sample (Table 4), when compared

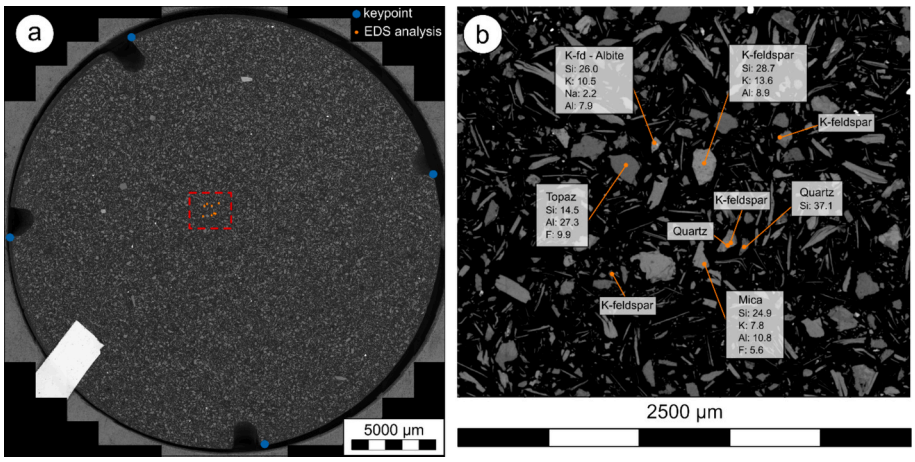

Fig. 10. (a) Identification of the reference points on the polished section (blue dots). EDS analysis to confirm the allocation of BSE colors to mineralogical phases (orange dots) (b) Focus on EDS analyses for mineral phase classification. (For interpretation of the references to colour in this figure legend, the reader is referred to the web version of this article.)

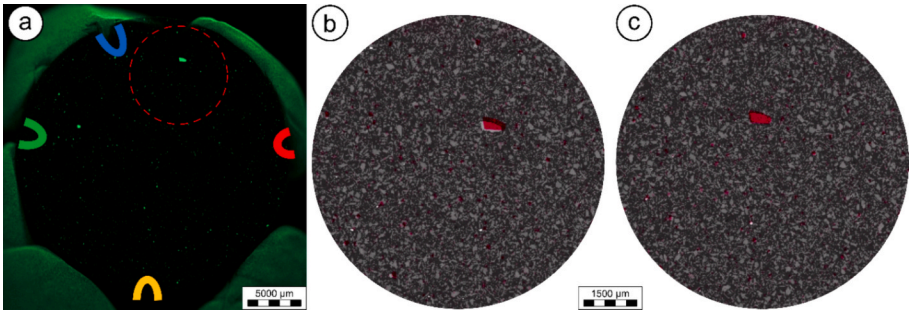

Fig. 11. (a) Ca elemental mapping along with the identification of the notches. Subtraction of the BSE image and the Ca mapping, the red grains represent the grains present in the Ca mapping in the case of (b) grains used as reference points and (c) notches used as reference points. (For interpretation of the references to colour in this figure legend, the reader is referred to the web version of this article.)

Table 4
Modal mineralogy obtained using the AMICS and MARCIA classification methods or calculated using EMC computation, based on the geochemistry of the sample.

Mineral	Quartz	Lepidolite	Muscovite	K-feldspar	Phosphate	Albite	Topaz
% – MARCIA	1.6	65.5	7.5	2.6	–	29.2	0
% – AMICS	4.2	68.5	16.6	2.8	–	7.2	0.6
% – EMC	5.0	57.0		0.6	–	8.4	22.57

to SEM-EDS used for AMICS. Using signal from µLIBS analysis could improve the classification of albite using MARCIA manual classification by adding mappings related to concentrations of fluorine and sodium.

4.3. Advantages of the developed method

4.3.1. Advantage of MARCIA for combining XRF and BSE

The key advantage of using the MARCIA Python code for processing fused data is its flexibility. This open-source classification tool provides an attractive alternative to commercial solutions. The data can be processed with MARCIA on any laptop, without internet connection.

The homography approach allows users to combine the most suitable analytical techniques for a given sample, offering a tailored and cost-effective alternative to commercial automated mineralogy solutions. Two main factors drive this cost efficiency. First, the equipment used is more affordable. µXRF is a recognized low-cost solution for elemental mapping, and since only micron-resolution BSE imaging is required, high-end instruments are unnecessary. Second, the total analysis time is reduced as BSE and µXRF mappings typically take about 2 to 3 h, which is faster than commercial automated mineralogy systems. The comparison of the different method is described in Table 5, which shows the advantages of each method. If AMICS can be faster regarding the post-processing time, MARCIA is flexible, a fast analytical time can be obtained if less analytical tools are combined, the post processing can be done on any laptop and the cost is reduced to the apparatus used. Finally, one parameter to consider is the need for MARCIA when data fusion has to been carried out, is to have a specific sample preparation in order to have key points identifiable on the sample.

Regarding MARCIA and the sample preparation, the use of markers, such as notches or other sample labels, makes it possible to automatically locate areas of interest, to be used for homography computation, prior to mapping. This enables semi-automatic image rescaling, making the method highly efficient once integrated into routine workflows. As a result, the data fusion process becomes straightforward and reliable.

Ultimately, for geological sample analysis, manual classification further enhances the method's adaptability. A geologist might focus on trace element distribution within minerals, while a mineral processing engineer may prioritize identifying and quantifying mineral phases and associations. This flexibility ensures the method meets diverse analytical needs with precision and control.

Table 5
Comparison of the processing times, cost and sample preparation procedures for AMICS and MARCIA.

Method	Analytical time (h)	Post-processing time	Post-processing facility	Cost	Sample preparation
AMICS	6 for the current study. The time depends on the size of the sample and resolution desired.	Several hours for the first classification then routine post-processing	Limited to workstations equipped with offline license	Apparatus + Software + Library	Depending on the apparatus
MARCIA data fusion	2 to 6 for the current study. The time depends on the methods combined.	Several hours for the first classification, then depending on the sample	Any workstation	Apparatus	Depending on the apparatus + Addition of the reference points on the sample

The use of a single integrated system to perform SEM, μXRF, and LIBS analyses in situ could theoretically be envisioned. However, such an approach faces substantial technical limitations. If the limitations regarding operating conditions, such as vacuum, can be overcome for the different methods (Sridhar et al., 2025; Thiem et al., 1994). Because LIBS is inherently destructive, SEM imaging (BSE/EDS) must be completed beforehand. Once the laser has ablated the surface, the same location cannot be reanalyzed by SEM.

Integrating multiple techniques into a single platform also poses challenges related to the precise spatial alignment of the analytical components (electron beam, laser beam, X-ray excitation), which must all access the same region of interest without interfering. Finally, relying on a single multi-modal instrument limits the analytical flexibility to the techniques available within that system. In contrast, using separate instruments preserves the ability to combine a wider range of complementary methods as needed. Some challenges that should be mentioned also include the bulkiness of the equipment with multi sensor, the maintenance of the different sensor, detectors, etc.

4.3.2. *The importance of the developed method and its flexibility*

Once the data fusion method has been established and validated, it can be applied to a wide array of challenges in geological sample analysis. One such challenge, explored in this study, involves the detection of light elements. The results demonstrated that conventional approaches, even when maximizing data extraction, were insufficient to reliably distinguish between lepidolite and muscovite. Resolving this required the introduction of a third, complementary analytical method (here LIBS).

Similarly, limitations related to the analysis depth of SEM and μXRF emerged during the study. To address this μLIBS was incorporated. Since LIBS relies on laser ablation, it provides surface-sensitive or consistent-depth analysis, offering valuable data that neither SEM nor μXRF could supply on their own, in the case of light elements bearing samples.

The combination of these complementary techniques illustrates the potential for integrating various types of analytical tools, elemental, molecular, or structural, within a unified data fusion framework. For example, one other possible perspective of this work is to implement in situ methods specific to crystallography, and thus, to minerals. Methods such as Raman (Tlili et al., 1989), infrared (Mekonenn, 2023) and Visible Near Infrared Short Wave Infrared (VNIR-SWIR) spectroscopies (Cardoso-Fernandes et al., 2021; Kim et al., 2021) seems particularly adapted to the identification of silicates, phosphates, calcium-bearing minerals and could help improving mineral processing stages. Such an approach opens new possibilities for advanced, multi-dimensional mapping tailored to the specific requirements of complex geological investigations.

4.4. *What about the separation process?*

4.4.1. *When looking at textures*

Fig. 9 illustrates several challenges related to optimizing lepidolite recovery: (i) mixed particles containing lepidolite are identifiable in a considerable number, suggesting that for this particle size fraction, liberation is not achieved; (ii) albite and potassium feldspar are abundantly found in the flotation concentrate. This suggests that flotation is not sufficiently selective towards these two minerals. The observation of this flotation concentrate suggests that the concentration of collector used may be too high, leading to the recovery of feldspar in the concentrate. Finally, it is worth noting that this flotation concentrate has a significant tin content (Table 3). Cassiterite may therefore not have been selectively separated from lepidolite. Thus, it is essential to find an alternative method to concentrate lepidolite without affecting the tin content, which is intended to be valorized in a separate stream. Several approaches are possible: (i) the use of different collectors, such as combinations of cationic and anionic collectors; (ii) the use of depressants, as tannin, lime, or barium chloride for the depression of cassiterite (Bulatovic, 2007; Wang, 2016; Wei et al., 2021; Zhang et al., 2023). It is also possible to modify the processing scheme by introducing a gravity separation step upstream of flotation, as has been done for the beneficiation of Yichun granite (China) (Liu, 2014).

One surprising clue to better understand limits of the process is the identification of quite coarse muscovite crystals in the sample (Fig. 9 c and d). This shows that (i) muscovite does not only occur as micro-muscovite and is thus not entirely eliminated during the desliming step and that (ii) flotation is not selective between lepidolite and muscovite crystals, limiting the maximum Li_2O grade obtained in the floated product, the theoretical maximum being 6.25 %Li_2O (Fig. 8). It should be considered that the initial muscovite and lepidolite content varies between 0–10 wt.% and 10–25 wt.%, respectively, depending on the location of the sample. One element to consider is also the close chemistry and crystallography of these two minerals. Muscovite could be found as intergrowth between lepidolite crystals (Choi et al., 2024; Punin et al., 1990). In that case, perfect liberation of lepidolite cannot be achieved and micro-muscovite is not fully removable through desliming.

4.4.2. *When using statistics given by mineralogical classifications*

Based on the developed method, 12 thin sections with various weathering degrees were submitted to lepidolite and muscovite content estimation. Lepidolite content can vary between 10 to 20 wt.% of the total content of the samples, whereas muscovite one varies between 0 to 10 wt.% (Kahou et al., 2024). However, the literature on flotation of lepidolite showed that separation of lepidolite and muscovite through flotation might be impossible to achieve (Korbel et al., 2023). Therefore, based on these assumptions, the theoretical maximum lithium grade that can be obtained in floated products, if the separation of lepidolite and muscovite from gangue minerals is perfect, is ranging from 3.12 to 6.20 %Li_2O, with its mean value being around 4.20 %Li_2O.

5. Conclusions

This study introduces an automated mineralogy methodological framework comprising two key components: (i) a characterization approach that integrates multiple mapping techniques using a homography matrix for spatial alignment and (ii) utilizes the MARCIA Python code to assign each pixel to a corresponding mineral phase. The method allows to characterize various samples, ranging from thin to polished sections submitted to physico-chemical separation processes. Challenges related to the superimposition of the images were overcome. In terms of mineralogical classification and textural analysis, the mineralogical mapping obtained using MARCIA and data fusion was compared to the

mineralogical mapping of the same sample obtained using a commercial automated mineralogy solution. The mappings display close mineralogical classification and textures. To further compare the two methods, the modal mineralogies obtained were compared to the one calculated by the element to mineral conversion method.

The developed method allows for a great flexibility as it is based on the combination of various characterization methods. The use of emerging methods such as μLIBS allows the analysis of the elemental distribution of light elements. This point remains crucial in the context of characterization of samples from the Beauvoir granite, a highly differentiate (Li, Be, F) granite. Finally, limits related to the spatial resolution of μLIBS and μXRF (~20 μm) compared to SEM (~1 μm) could be overcome by interpolating experimental data, in order to resize the μLIBS and μXRF mappings to the resolution of the BSE imaging. Adding automated in situ analysis method could be easily practicable and could allow for a supplementary characterization precision. Ultimately, this study, which integrates various analytical methods, opens promising avenues in mineral processing by enabling more precise characterization of complex samples containing light elements bearing minerals. These advancements are expected to significantly improve ore characterization and mineral processing of complex light bearing elements ores.

CRediT authorship contribution statement

C. Korbel: Writing – original draft, Methodology, Investigation, Data curation, Conceptualization. **B. Demeusy:** Methodology, Investigation, Data curation. **Z.S. Kahou:** Writing – review & editing, Methodology, Investigation, Data curation, Conceptualization. **C. Fabre:** Writing – review & editing, Validation, Supervision, Methodology, Investigation, Data curation. **V. Motto-Ros:** Writing – review & editing, Validation, Methodology, Investigation, Data curation. **Y. Teitler:** Writing – review & editing, Validation, Supervision, Methodology, Conceptualization. **L. Salsi:** Validation, Methodology, Investigation. **A. Lecomte:** Writing – review & editing, Validation, Methodology, Investigation, Data curation. **I.V. Filippova:** Writing – review & editing, Supervision. **L.O. Filippov:** Writing – review & editing, Supervision. **J. Cauzid:** Writing – review & editing, Validation, Supervision, Methodology, Conceptualization.

Declaration of competing interest

The authors declare that they have no known competing financial interests or personal relationships that could have appeared to influence the work reported in this paper.

Acknowledgment

The authors acknowledge the financial support from Labex Ressources 21 supported by the French National Research Agency through the national program “Investissements d’Avenir” [reference ANR–10–LABX–0021]. This research received partial funding from the European Union’s Framework programme for Research and Innovation Horizon Europe under Grant agreement 101091543. This work was partially supported by the French region Rhônes Alpes Auvergne (Optolyse, CPER2016). Experiments leading to this publication were performed at the STEVAL (Station Expérimentale de Valorisation des ressources minérales et des substances residuaires) facility and the SCMEM (Service Commun de Microscopie Electronique et Microanalyse X) facilities of the GeoRessources research centre (Université de Lorraine and CNRS). The authors also acknowledge Arnaud Marotel for producing the notches onthe polished sections.

Appendix A. Supplementary data

Supplementary data to this article can be found online at https://doi.org/10.1016/j.mineng.2026.110158.

Data availability

Data will be made available on request.

References

Alvarez-Llamas, C., Tercier, A., Ballouard, C., Fabre, C., Hermelin, S., Margueritat, J., Duponchel, L., Dujardin, C., Motto-Ros, V., 2024. Ultrafast μLIBS imaging for the multiscale mineralogical characterization of pegmatite rocks. J. Anal. At. Spectrom 39, 1077–1086.

Aubert, G., 1969. Les coupoles granitiques de Montebras et d’Echassieres (Massif central francais) et la genese de leurs mineralisations en etain, lithium, tungstene et beryllium. Ed. du Bureau de recherches geologiques et minieres.

Ayoub, F., Leprince, S., Avouac, J.-P., 2009. Co-registration and correlation of aerial photographs for ground deformation measurements. ISPRS J. Photogramm. Remote Sens. 64, 551–560.

Barker, R.D., Barker, S.L.L., Wilson, S., Stock, E.D., 2021. Quantitative mineral mapping of drill core surfaces I: a method for μ XRF mineral calculation and mapping of hydrothermally altered, fine-grained sedimentary rocks from a carlin-type gold deposit. Econ. Geol. 116, 803–819. https://doi.org/10.5382/econgeo.4803.

Behling, R., Roessner, S., Segl, K., Kleinschmit, B., Kaufmann, H., 2014. Robust automated image co-registration of optical multi-sensor time series data: database generation for multi-temporal landslide detection. Remote Sens. (Basel) 6, 2572–2600.

Berthou, W., Legallais, M., Bousquet, B., Motto-Ros, V., Le Cras, F., 2024. Characterization of lithium phosphorus oxide thin film libraries by laser-induced breakdown spectroscopy imaging: a step towards high-throughput quantitative analyses. Spectrochim. Acta B At. Spectrosc. 215, 106906.

Boucif, R., Filippov, L.O., Maza, M., Benabdeslam, N., Foucaud, Y., Marin, J., Korbel, C., Demeusy, B., Diot, F., Bouzidi, N., 2024. Optimizing liberation of phosphate ore through high voltage pulse fragmentation. Powder Technology 437, 119549.

Bradley, D.C., McCauley, A.D., Stillings, L.M., 2017. Mineral-Deposit Model for Lithium-CesiumTantalum Pegmatites, in: Mineral Deposit Models for Resource Assessment, Scientific Investigations Report.

Buchmann, M., Schach, E., Tolosana-Delgado, R., Leißner, T., Astoveza, J., Kern, M., Möckel, R., Ebert, D., Rudolph, M., van den Boogaart, K., Peuker, U., 2018. Evaluation of magnetic separation efficiency on a cassiterite-bearing skarn ore by means of integrative SEM-based image and XRF–XRD data analysis. Minerals 8, 390. https://doi.org/10.3390/min8090390.

Bulatovic, S.M., 2007. Handbook of flotation reagents: chemistry, theory and practice, 1st ed. Elsevier, Amsterdam, Boston.

Cáceres, J.O., Pelascini, F., Motto-Ros, V., Moncayo, S., Trichard, F., Panczer, G., Marín-Roldán, A., Cruz, J.A., Coronado, I., Martín-Chivelet, J., 2017. Megapixel multi-elemental imaging by Laser-Induced Breakdown Spectroscopy, a technology with considerable potential for paleoclimate studies. Sci. Rep. 7, 5080. https://doi.org/10.1038/s41598-017-05437-3.

Capela, D., Lopes, T., Dias, F., Ferreira, M.F., Teixeira, J., Lima, A., Jorge, P.A., Silva, N. A., Guimarães, D., 2025. Advancing automated mineral identification through LIBS imaging for lithium-bearing mineral species. Spectrochim. Acta B At. Spectrosc. 223, 107085.

Cardoso-Fernandes, J., Silva, J., Perrotta, M.M., Lima, A., Teodoro, A.C., Ribeiro, M.A., Dias, F., Barrès, O., Cauzid, J., Roda-Robles, E., 2021. Interpretation of the reflectance spectra of lithium (Li) minerals and pegmatites: a case study for mineralogical and lithological identification in the Fregeneda-Almendra area. Remote Sens. (Basel) 13, 3688. https://doi.org/10.3390/rs13183688.

Charoy, B., 1999. Beryllium speciation in evolved granitic magmas; phosphates versus silicates. Eur. J. Mineral. 11, 135–148.

Choi, W., Park, C., Heo, C.-H., Yang, S.-J., Oh, I.-H., Park, K.S., Choi, S.H., 2024. Magmatic to aqueous phase transition in Li-pegmatite: microtextural and geochemical study of muscovite–lepidolite from Boam mine area, Uljin, South Korea. Miner. Deposita 59, 1641–1660.

Cuney, M., Marignac, C., Weisbrod, A., 1992. The Beauvoir topaz-lepidolite albite granite (Massif Central, France); the disseminated magmatic Sn-Li-Ta-Nb-Be mineralization. Econ. Geol. 87, 1766–1794. https://doi.org/10.2113/gsecongeo.87.7.1766.

European Commission, 2023. Study on the critical raw materials for the EU 2023 – Final report. Publications Office of the European Union. https://doi.org/10.2873/725585.

Fabre, C., Boiron, M.-C., Dubessy, J., Chabiron, A., Charoy, B., Martin Crespo, T., 2002. Advances in lithium analysis in solids by means of laser-induced breakdown spectroscopy: an exploratory study. Geochim. Cosmochim. Acta 66, 1401–1407. https://doi.org/10.1016/S0016-7037(01)00858-4.

Fabre, C., Devismes, D., Moncayo, S., Pelascini, F., Trichard, F., Lecomte, A., Bousquet, B., Cauzid, J., Motto-Ros, V., 2018. Elemental imaging by laser-induced breakdown spectroscopy for the geological characterization of minerals. J. Anal. At. Spectrom 33, 1345–1353.

Fandrich, R., Gu, Y., Burrows, D., Moeller, K., 2007. Modern SEM-based mineral liberation analysis. Int. J. Miner. Process. 84, 310–320. https://doi.org/10.1016/j.minpro.2006.07.018.

Flude, S., Haschke, M., Storey, M., 2017. Application of benchtop micro-XRF to geological materials. Mineral. Mag. 81, 923–948.

Gallhofer, D., Lottermoser, B., 2018. The influence of spectral interferences on critical element determination with portable X-ray fluorescence (pXRF). Minerals 8, 320. https://doi.org/10.3390/min8080320.

Gu, Y., Napier-Munn, T., 1997. JK/Philips mineral liberation analyzer–an introduction, in: Minerals Processing '97 Conf. Cape Town, AS.
Gu, Y., Schouwstra, R.P., Rule, C., 2014. The value of automated mineralogy. Miner. Eng. 58, 100–103. https://doi.org/10.1016/j.mineng.2014.01.020.
Haschke, M., 2014. Laboratory micro-X-ray fluorescence spectroscopy: instrumentation and applications, Springer Series in Surface Sciences. Springer International Publishing, Cham. Doi: 10.1007/978-3-319-04864-2.
Jeong, G.Y., 2008. Bulk and single-particle mineralogy of Asian dust and a comparison with its source soils. J. Geophys. Res. 113, D02208. https://doi.org/10.1029/2007JD008606.
Jiao, Y., Qiu, K.-H., Zhang, P.-C., Li, J.-F., Zhang, W.-T., Chen, X.-F., 2020. Process mineralogy of Dalucao rare earth ore and design of beneficiation process based on AMICS. Rare Met. 39, 959–966. https://doi.org/10.1007/s12598-020-01446-w.
Kahou, S., Cathelineau, M., Boiron, M.-C., 2024. Quantitative mineralogy and lithium distribution in the upper part of the Beauvoir granite. Presented at the EGU General Assembly 2024, Copernicus Meetings, Vienna. Doi: 10.5194/egusphere-egu24-1668.
Kaskes, P., Déhais, T., de Graaff, S.J., Goderis, S., Claeys, P., 2021. Micro–X-ray fluorescence (μXRF) analysis of proximal impactites: High-resolution element mapping, digital image analysis, and quantifications. In: Reimold, W.U., Koeberl, C. (Eds.), Large Meteorite Impacts and Planetary Evolution VI. Geological Society of America, pp. 171–206. https://doi.org/10.1130/2021.2550(07).
Kim, Y., Caumon, M.-C., Barres, O., Sall, A., Cauzid, J., 2021. Identification and composition of carbonate minerals of the calcite structure by Raman and infrared spectroscopies using portable devices. Spectrochim. Acta A Mol. Biomol. Spectrosc. 261, 119980. https://doi.org/10.1016/j.saa.2021.119980.
Korbel, C., Demeusy, B., Kahou, Z.S., Filippova, I.V., Dehaine, Q., Filippov, L.O., 2025. Flowsheet development for the selective flotation of lepidolite from the Beauvoir granite from mineralogical insights. Miner. Eng. 225, 109207.
Korbel, C., Filippova, I., Filippov, L., 2023. Froth flotation of lithium micas–a review. Miner. Eng. 192, 107986.
Korbel, C., Mezoued, N., Demeusy, B., Fabre, C., Cauzid, J., Filippova, I., Filippov, L., 2024. Quantification of lithium using handheld instruments: application of LIBS and XRF spectroscopy to assay the lithium content of mineral processing products. J. Anal. At. Spectrom. https://doi.org/10.1039/D3JA00423F.
Kosakevitch, A., 1976. Evolution de la minéralisation en Li, Ta et Nb dans la coupole granitique de Beauvoir (massif d'Echassières, Allier). Rapport BRGM 76.
Kupka, N., Tolosana-Delgado, R., Schach, E., Bachmann, K., Heinig, T., Rudolph, M., 2020. R as an environment for data mining of process mineralogy data: a case study of an industrial rougher flotation bank. Miner. Eng. 146, 106111. https://doi.org/10.1016/j.mineng.2019.106111.
Lacroix, E., Cauzid, J., Teitler, Y., Cathelineau, M., 2021. Near real-time management of spectral interferences with portable X-ray fluorescence spectrometers: application to Sc quantification in nickeliferous laterite ores. GEEA 21, geochem2021-015. https://doi.org/10.1144/geochem2021-015.
Lagache, M., Quemeneur, J., 1997. The Volta Grande Pegmatites, Minas Gerais, Brazil: an example of rare-element granitic pegmatites exceptionally enriched in lithium and rubidium. Can. Mineral. 35, 153–165.
Lee, D.-H., Han, S.-C., Kim, T.-H., Yun, J.-I., 2011. Highly sensitive analysis of boron and lithium in aqueous solution using dual-pulse laser-induced breakdown spectroscopy. Anal. Chem. 83, 9456–9461. https://doi.org/10.1021/ac2021689.
Li, Y., Le Pape, Y., Rodriguez, E.T., Torrence, C.E., Mena, J.A., Rosseel, T.M., Sircar, M., 2020. Microstructural characterization and assessment of mechanical properties of concrete based on combined elemental analysis techniques and Fast-Fourier transform-based simulations. Constr. Build. Mater. 257, 119500.
Liu, Y.-L., 2014. The FlotationProcess of Lepidolite in Jiangxi Province in China 5.
Longerich, H.P., Jackson, S.E., Günther, D., 1996. Inter-laboratory note. Laser ablation inductively coupled plasma mass spectrometric transient signal data acquisition and analyte concentration calculation. J. Anal. At. Spectrom 11, 899–904.
Maragh, J.M., 2021. A multiscale framework for the chemomechanical characterization of ancient heterogeneous materials. Massachusetts Institute of Technology.
Mekonenn, S.A., 2023. Spectral analysis of lithium-bearing micas with shortwave and longwave infrared spectroscopy. University of Twente.
Menzies, A.H., Tagle, R., Reinhardt, F., Hirschle, C., Schellkopf, L.J., Kelly, N., 2022. High-speed micro-XRF analysis of rock samples and drill cores. Microsc. Microanal. 28, 650–651. https://doi.org/10.1017/S1431927622003117.
Meyer, H., Cauzid, J., 2021. MARCIA.
Nardecchia, A., Fabre, C., Cauzid, J., Pelascini, F., Motto-Ros, V., Duponchel, L., 2020. Detection of minor compounds in complex mineral samples from millions of spectra: a new data analysis strategy in LIBS imaging. Anal. Chim. Acta 1114, 66–73. https://doi.org/10.1016/j.aca.2020.04.005.
Neukampf, J., Ellis, B.S., 2025. Lithium loss from pegmatites controlled by country rock temperature. Nat. Commun. 16, 448. https://doi.org/10.1038/s41467-024-55794-7.
Nikonow, W., Rammlmair, D., 2017. Automated mineralogy based on micro-energy-dispersive X-ray fluorescence microscopy (μ-EDXRF) applied to plutonic rock thin sections in comparison to a mineral liberation analyzer. Geosci. Instrum. Method. Data Syst. 6, 429–437. https://doi.org/10.5194/gi-6-429-2017.
Ortiz Ortega, E., Hosseinian, H., Rosales López, M.J., Rodríguez Vera, A., Hosseini, S., 2022. Characterization techniques for morphology analysis, in: Material Characterization Techniques and Applications. Springer, pp. 1–45.
Parian, M., Lamberg, P., Möckel, R., Rosenkranz, J., 2015. Analysis of mineral grades for geometallurgy: combined element-to-mineral conversion and quantitative X-ray diffraction. Miner. Eng. 82, 25–35. https://doi.org/10.1016/j.mineng.2015.04.023.
Pereira, L., Birtel, S., Möckel, R., Michaux, B., Silva, A.C., Gutzmer, J., 2019. Constraining the economic potential of by-product recovery by using a geometallurgical approach: the example of rare earth element recovery at Catalão I, Brazil. Econ. Geol. 114, 1555–1568. https://doi.org/10.5382/econgeo.4637.
Pirrie, D., Rollinson, G.K., 2011. Unlocking the applications of automated mineral analysis. Geol. Today 27, 226–235.
Pollard, P.J., 1995. A special issue devoted to the geology of rare metal deposits; geology of rare metal deposits; an introduction and overview. Econ. Geol. 90, 489–494.
Potts, P.J., 1992. A Handbook of Silicate Rock Analysis. Springer US, Boston, MA. Doi: 10.1007/978-1-4615-3270-5.
Punin, Y.O., Kotel'nikova, Y.N., Sokolov, P.B., Kretser, Y.L., Semina, Y.Y., 1990. Polytype intergrowths of lithium micas. International Geology Review 32, 13–22.
Sandmann, D., 2015. Method Development in Automated Mineralogy. Fakultät für Geowissenschaften, Geotechnik und Bergbau der Technischen Universität Bergakademie Freiberg.
Scheller, S., Tagle, R., Gloy, G., Barraza, M., Menzies, A., 2017. Advancements in minerals identification and characterization in geo-metallurgy: comparing E-beam and micro-X-ray-fluorescence technologies. Microsc. Microanal. 23, 2168–2169. https://doi.org/10.1017/S1431927617011503.
Sridhar, R., Malathi, S., Kumar, S., Roy, U.M., Sriram, K.V., 2025. Investigation of LE-LIBS feasibility for detection of H, He, and O in high vacuum using geological samples. Opt. Lett. 50, 1500–1503.
Sutherland, D.N., Gottlieb, P., 1991. Application of automated quantitative mineralogy in mineral processing. Miner. Eng. 4, 753–762. https://doi.org/10.1016/0892-6875(91)90063-2.
Thiem, T.L., Salter, R.H., Gardner, J.A., Lee, Y.I., Sneddon, J., 1994. Quantitative simultaneous elemental determinations in alloys using laser-induced breakdown spectroscopy (LIBS) in an ultra-high vacuum. Appl. Spectrosc. 48, 58–64.
Tjallingii, R., Röhl, U., Kölling, M., Bickert, T., 2007. Influence of the water content on X-ray fluorescence core-scanning. Geochem. Geophys. Geosyst. 8. https://doi.org/10.1029/2006GC001393.
Tlili, A., Smith, D.C., Beny, J.-M., Boyer, H., 1989. A Raman microprobe study of natural micas. Mineral. Mag. 53, 165–179. https://doi.org/10.1180/minmag.1989.053.370.04.
Tolosana-Delgado, R., von Eynatten, H., Karius, V., 2011. Constructing modal mineralogy from geochemical composition: a geometric-Bayesian approach. Comput. Geosci. 37, 677–691. https://doi.org/10.1016/j.cageo.2010.08.005.
Tonžetić, I., 2017. Micro-XRF: A New Automated Mineralogical Analysis Paradigm. Presented at the Process Mineralogy, Cape Town, South Africa.
Vanderbruggen, A., Gugala, E., Blannin, R., Bachmann, K., Serna-Guerrero, R., Rudolph, M., 2021. Automated mineralogy as a novel approach for the compositional and textural characterization of spent lithium-ion batteries. Miner. Eng. 169, 106924. https://doi.org/10.1016/j.mineng.2021.106924.
Wang, D., 2016. Depressants, in: Flotation Reagents: Applied Surface Chemistry on Minerals Flotation and Energy Resources Beneficiation. Springer Singapore, Singapore, pp. 125–144. Doi: 10.1007/978-981-10-2027-8_4.
Wei, Q., Feng, L., Dong, L., Jiao, F., Qin, wenqing, 2021. Selective co-adsorption mechanism of a new mixed collector on the flotation separation of lepidolite from quartz 9.
Wills, B.A., Finch, J., 2015. Wills' mineral processing technology: an introduction to the practical aspects of ore treatment and mineral recovery. Butterworth-heinemann.
Yang, J., Zhang, Z., Cheng, Q., 2022. Resolution enhancement in micro-XRF using image restoration techniques. J. Anal. At. Spectrom 37, 750–758.
Zhang, X., Tan, X., Li, C., Yi, Y., Liu, W., Zhang, L., 2019. Energy-efficient and simultaneous extraction of lithium, rubidium and cesium from lepidolite concentrate via sulfuric acid baking and water leaching. Hydrometall. 185, 244–249. https://doi.org/10.1016/j.hydromet.2019.02.011.
Zhang, Z., Wei, Q., Jiao, F., Qin, W., 2023. Role of nanobubbles on the fine lepidolite flotation with mixed cationic/anionic collector. Powder Technol. 427, 118785. https://doi.org/10.1016/j.powtec.2023.118785.